Cleaner Engineering and Technology 32 (2026) 101214

Contents lists available at ScienceDirect

Cleaner Engineering and Technology

journal homepage: www.sciencedirect.com/journal/cleaner-engineering-and-technology

Clean production of biochar-based sustainable lightweight PCM composites: Effect of pyrolysis parameters on thermal and energy storage

Karuppiah Theriselvam [a], Arumugaprabu Veerasimman [a,*], Flavio Stochino [b,**], Arnas Majumder [b]

[a] Department of Mechanical Engineering, Kalasalingam Academy of Research and Education, Krishnankovil, Srivilliputhur, 626126, India
[b] Department of Civil Environmental Engineering and Architecture, University of Cagliari, via Marengo 2, Cagliari, CA, 09123, Italy

ARTICLE INFO

Keywords:
Phase change material
Biomass
Low cost composites
Renewable energy
Leak- proof
Thermal conductivity

ABSTRACT

In recent years, many strategies have been developed to prevent Phase change material (PCM) leakage, but it remains a major challenge to develop PCMs with the advantages of low production costs, sustainability, reusability, and the use of fillers made from waste biomass. Paraffin wax, an organic Phase change material, was used as a thermal storage material. To reduce the total cost of production and produce inexpensive biochar, biomass extracted from the root of the *Prosopis juliflora* plant was subjected to a pyrolysis process with low oxygen and without the use of inert gases. In order to investigate the PCM adsorption properties of the biochar, two types of biochars, PJR 400 and PJR 500, were prepared by varying the pyrolysis temperature to 400 °C and 500 °C. Then, using the direct impregnation technique, this biochar was blended with PCM at various weight percentages, i.e. 5%, 15%, 25%, 35%, and 45%. The surface area values of PJR500 and PJR400 biochars prepared at two different temperatures were found to be 4.451 and 2.423 m^2/g, respectively. After Brunauer-Emmett-Teller (BET) analysis, SEM, XRD and FTIR measurements were used to analyze and verify the morphological and chemical properties of the PCM blends and biochars. DSC, thermal conductivity and leakage studies were conducted to determine the performance and heat storage capacity of the PCM, and the results were compared. In addition to preventing leakage, the PJR 500 biochar blend with PCM at 45% also had thermal conductivity and heat storage enthalpy values of 90.24 J/g and 0.463 W/mk, respectively.

1. Introduction

The demand for energy worldwide is increasing day by day. As of now, all countries are forced to use more natural resources to meet their needs due to their country's development and population growth. Apart from this, natural resources are being imported through agreements with neighbouring countries and natural resources are being exploited day by day on a global scale. The Earth is facing climate changes such as global warming, increased rainfall, and drought due to the daily use of natural resources. In the current situation, all countries of the world are increasingly promoting the use of renewable energy for energy needs. Numerous studies are being conducted to meet the energy demand using natural renewable sources such as wind, water, and sunlight. For example, a renewable resource material with heat energy storage and release properties is required to store heat energy for various applications such as electronic device cooling, building temperature control, solar dryer, waste heat recovery, and food processing. In this way, Phase change material (PCM) can be used as a renewable resource material for applications such as heat energy storage and release. Phase change materials can be used as a thermal energy storage devices due to their properties such as steady phase transition temperature, high storage capacity, stability, and ease of use (Mandal et al., 2022; Liu and Yang, 2015; Farid et al., 2021; Agyenim et al., 2010). When PCM is heated to its melting point temperature, it changes from a solid to a liquid, absorbing heat from the surroundings. When the temperature drops below the melting point temperature of PCM, it releases the stored heat to the surroundings and turns into a solid (Assareh et al., 2024; Amini et al., 2023; Mohammed et al., 2024). The heat stored and released is considered as latent heat. The heat stored in PCM is stored in two ways: latent heat and sensible heat, however, the heat energy stored through latent heat is stored more than the heat energy stored through sensible heat (Barzin et al., 2015; Bahadori and Haghighat, 1985; Arteconi et al.,

* Corresponding author.
** Corresponding author.
E-mail addresses: v.arumugaprabu@klu.ac.in (A. Veerasimman), flavio.stochino@unica.it (F. Stochino).

https://doi.org/10.1016/j.clet.2026.101214
Received 25 November 2025; Received in revised form 21 March 2026; Accepted 21 April 2026
Available online 25 April 2026

2012). PCMs can be divided into three types: organic, inorganic, and eutectic PCM (Mandal et al., 2022; Sun et al., 2013; Liu and Yang, 2016; Huang et al., 2013). The use of PCM has been hindered by reasons such as low phase change enthalpy and thermal conductivity, poor phase segregation and phase separation, sub cooling, and corrosion (Saffari et al., 2017; Zalba et al., 2003; Mehling and Cabeza, 2008). Apart from this, PCM can be divided into different types depending on its melting point temperature (Noohi et al., 2022; Cárdenas and León, 2013; Costa and Kenisarin, 2022; Ge et al., 2013). Paraffin wax is one of the organic PCMs. It is available in different melting point temperatures to suit different applications. Paraffin wax is widely used in heating and electrical applications due to its melting point temperature range (Murali et al., 2024; Asbik et al., 2016, 2021; Kabeel et al., 2020). This liquid phase will leak out of the structure if the PCM is not chemically stabilized or physically contained inside a porous matrix, resulting in material loss and decreased heat storage capacity. Additionally, the use of paraffin wax in thermal management control applications is restricted when it is used directly with materials because of issues like low thermal conductivity, poor adhesion, decreased mechanical strength, increased leakage, and loss of material integrity (Lucas et al., 2013; Pasupathy et al., 2008). Therefore, current studies focus more on claims such as changes in latent heat enthalpy and prevention of leakage by changing the design structure and thermal properties of PCM (Pomianowski et al., 2013; Zhang et al., 2006; Kousksou et al., 2010). Consequently, a composite structure must be transformed into shape-stabilized PCM in order to stop PCM from leaking. Such a composite structure must have a higher thermal conductivity value than pure PCM. By increasing the thermal conductivity value, the heat releasing and absorbing rate of the composite PCM increases. By converting shape stabilized PCM into composite, leakage is prevented when PCM is injected into a porous material through micro encapsulation technique (Lucas et al., 2013; Boh and Šumiga, 2008). PCM can be infused with a variety of materials to form shape stabilized PCM. For example, polymers (Qu et al., 2018; Aydın and Okutan, 2013; Karaman et al., 2011), metallic foams (Oya et al., 2012; Xiao et al., 2013, 2014), and carbon nanostructure materials (Stonehouse and Abeykoon, 2022; Hashempour and Vakili, 2018) can be used for microencapsulation. However, the high cost, complex manufacturing process, and environmental impact of the above materials make their use difficult. Graphene/CNTs have a very small number of pores, which requires additional closure layers (Du et al., 2026). Therefore, they are less capable of stabilizing molten PCM. Although metal foam has high porosity, it has a large number of macropores (>100 μm) (Saeed et al., 2022). In this case, there is a risk of leakage due to the weak capillary force between the pores. In previous studies, biochar was obtained from biomass such as wood biochar, agricultural waste, seeds/shells, and wood dust/husk and was shaped by combining it with phase change materials. As a result, it is many times cheaper. In addition, biochar's highly porous structure, high carbon content, economical and lightweight nature serve as a solution to these problems (KÖSE, 2023; Jeon et al., 2019; Sarı et al., 2020; Can and Żigon, 2022). However, although various studies have been conducted on biomasses, the retention properties of biochar, such as surface area, pore size, and pore volume, vary depending on the biomass. Below are the surface characteristics of biochars derived from natural sources that have been studied in the past. The surface area and average pore width values of neem seed 300 biochar were calculated to be 0.481 m^2/g and 10.229 nm, respectively (Mandal et al., 2026). Biochar obtained from corn stalks without any activation method showed a surface area of 13.71 m^2/g and a pore diameter of 10.072 nm (Huang et al., 2026). The surface area and pore diameter values of biochar obtained by activating rice husk with KOH were found to be 289.220 m^2/g and 10.198 nm, respectively (Huynh et al., 2026). Among these, pyrolysis temperature is an important factor in modifying the surface properties of biochar. Although numerous studies have affected the surface properties of biochar by varying the pyrolysis temperature, they have not been used for phase change material applications. In this study, the root part of the plant Noval *Prosopis juliflora* was selected as the biomass, and the pyrolysis temperature was set at 400 °C and 500 °C, and the two biochars obtained were shown to absorb paraffin wax.

Paraffin wax, with a melting point between 58 °C and 62 °C, was used as a phase change material (PCM) for thermal energy storage. Biochar produced by pyrolysis of *Prosopis juliflora* root biomass was used to convert PCM into a shape-stabilized composite. Pyrolysis process parameters, including heating rate, temperature, residence time, inert gas type, and furnace type, affect the physicochemical properties of the biochar and the properties of the final product. In this study, biochar was produced by oxidative pyrolysis in a muffle furnace without inert gas, which is an important parameter in pyrolysis processes. To investigate the effect of temperature, oxidative pyrolysis produces two distinct types of biochar at 400 °C and 500 °C. Paraffin wax was formed into shape-stabilized composites with these biochars by a simple impregnation technique. This study shows how increasing the pyrolysis temperature to 400 and 500 °C changes the surface properties of biochar. The study also reveals how these two types of biochar influence the heat storage capacity of PCM. It identifies which weight percentage of biochar offers the best combination of thermal conductivity, leakage resistance, thermal stability, and heat storage value, ultimately promoting PCM performance. The resulting composites are designed for thermal management in device enclosures, electronic battery packs, and heat-sensitive materials. These composites have a melting point of 58 °C, which prevents overheating and maintains a stable temperature during use.

2. Materials and methods

2.1. Materials

Although paraffin has different melting point temperatures, paraffin wax, with a melting point temperature of 58–62 Celsius, was used as a heat storage material in this study, especially for applications such as electronics cooling and solar dryers. The density value of the wax with a long hydrocarbon chain was 0.88 g/cm^3. It was obtained from Royal Scientific Solutions, a chemical company in Tamil Nadu, India. The root part of the prosopis juliflora plant, which is the biomass used to make biochar, was obtained from Noorullaa Saw Mill in Sriviiliilputtur, Tamil Nadu.

2.2. Impregnation of PCM into biochar

Fig. 1 shows the overall production process of the shape-stabilized composites. Roots from *Prosopis juliflora* trees, cut into 30 cm lengths, were placed in a hot air oven at 120 °C for about 8 h to remove moisture. Biochar was then prepared using oxidative pyrolysis, without inert gas, in a muffle furnace at two temperatures: 400 °C and 500 °C. Pyrolysis parameters included a heating rate of 5 °C/min and a holding time of 100 min, both affecting the thermophysical properties of the biochar. Biochar produced at 400 °C was named PJR400, and biochar from 500 °C was called PJR500. Each sample was finely ground using a ball mill and sieved to obtain particles not exceeding 300 μm. Paraffin wax in pellet form, with a melting point of 58 °C, was melted at 70 °C. The two biochars, once converted into powders, were separately mixed with liquid paraffin wax in weight percentages of 5%, 15%, 25%, 35%, and 45%. Mixing was done for about 2 h using a mechanical stirrer while keeping the temperature at 70 °C, above the melting point of paraffin wax. The PCM and biochar mixtures were then placed in a vacuum pump and a hot air oven for about 60 min at a vacuum pressure of 20 Hg and a temperature of 70 °C. Thus, both biochars were combined with varying amounts of melted paraffin wax using a simple impregnation technique. The symbol PW0 indicates paraffin wax. The impregnated composite samples of biochar at 400 °C were designated as PWPJR4005, PWPJR40015, PWPJR40025, PWPJR40035, and PWPJR40045. Similarly, the composite samples at 500 °C were designated as PWPJR5005,

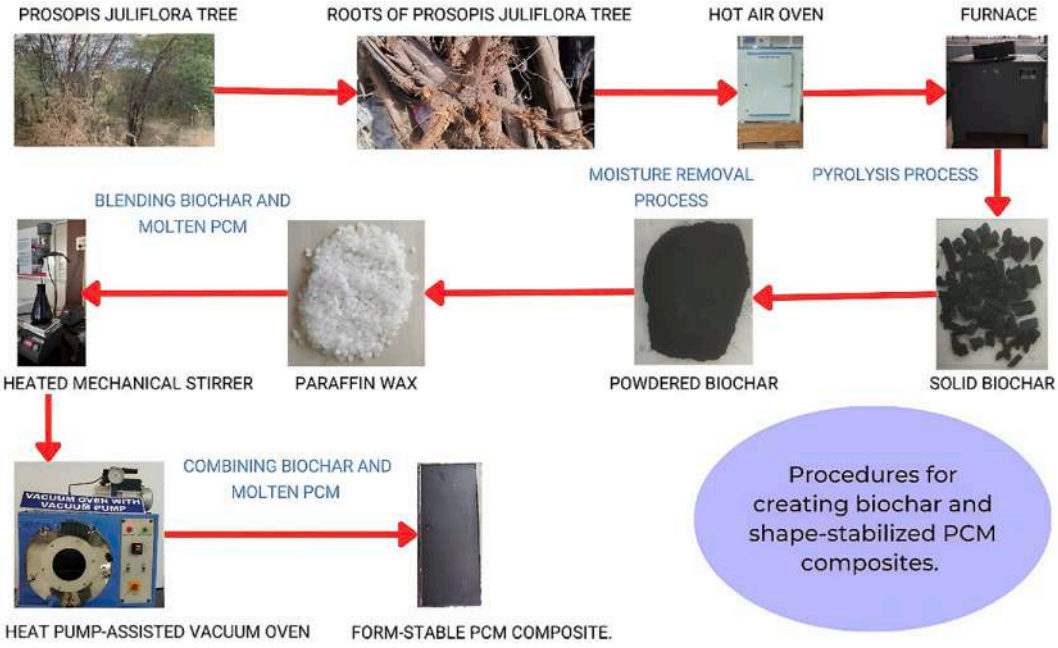

Fig. 1. Preparation method for bonded shape-stabilized composite using a simple impregnation technique.

PWPJR50015, PWPJR50025, PWPJR50035, and PWPJR50045.

3. Result and discussion

3.1. EDAX analysis of biochar

For the compounds, characteristic elements were identified by an EDAX-energy dispersive X-ray analysis system equipped with SDD (silicon drift detection) and an intermediate SEM platelet. Measurements were performed with the probe set at 15 kV, the working distance adjusted to ~10 mm (minimum), and direct acquisition times of 60–120 s. Looking closely at Tables 1 and 2 in the EDAX study, minerals such as Al, K, and Ca are found to be present in elemental analysis, each in amounts less than 1%. As expected, carbon has the highest weight percentage in both types of biochar, followed by oxygen to some extent. Since biochar is prepared using the oxidative pyrolysis method, no inert gas is formed. Comparing the two biochars, PJR500 biochar has a higher carbon weight percentage than PJR400 biochar.

From this, it can be observed that carbon production increases as the temperature rises. Simultaneously, the weight percentage of minerals also increases significantly with rising temperature. Looking closely at the PJR500 biochar Table 2, the aluminium disappears as the temperature rises. Minerals such as calcium and potassium contribute to the structural stability of biochar. Additionally, calcium has the ability to absorb carbon dioxide from the atmosphere (Mesnage et al., 2025), making it an eco-friendly biochar. Furthermore, calcium and potassium possess high adsorption properties (Bose et al., 2022), making the porous structure of biochar suitable for absorbing PCM. If calcium and oxygen are present, there is a high likelihood of limestone formation

Table 1
Assessment of the constituent's composition of PJR400 biochar.

S.NO	Element	Weight %	Atomic %	Error %	K ratio
1	C K	79.0	84.4	4.1	0.5839
2	O K	18.2	14.6	14.1	0.0221
3	AlK	0.5	0.2	10.7	0.0033
4	ClK	0.3	0.1	30.0	0.0029
5	K K	0.9	0.3	13.0	0.0079
6	CaK	1.0	0.3	18.2	0.0092

Table 2
Assessment of the constituent's composition of PJR500 biochar.

S.NO	Element	Weight %	Atomic %	Error %	K ratio
1	C K	85.9	91.5	3.8	0.6648
2	O K	8.1	6.5	17.9	0.0085
4	ClK	0.8	0.3	21.7	0.0068
5	K K	2.6	0.8	11.6	0.0227
6	CaK	2.6	0.8	9.9	0.0230

(Iacomino et al., 2024). The chlorine content is slightly higher in PJR500. In general, chlorine has strong corrosive properties. However, since it is present in low amount in biochar, the risk of significant corrosion damage during use is minimal.

3.2. SEM analysis of biochar

Using a Carl Zeiss EVO 18 scanning electron microscope, the porous structure of biochar was examined in terms of surface structure and cross-sectional area. The EVO 18's voltage range of 0.2–30 kV enables exact observation of the material's structure by providing precision control over the radiation's penetration depth and surface sensitivity. From the SEM Fig. 4a–d, it is clear that both biochars have a porous structure, although the difference between the two biochars becomes apparent as the temperature increases. As shown in the below Fig. 2 (b), internal pores are visible in the porous structure of PJR400 biochar, whereas they are absent in PJR500. It has a red marking on it.

These internal pores have been eliminated due to the rise in temperature. In Fig. 2a and b, numerous micro and meso pores appear. The varied surface morphology indicates that the biochar has a clear, porous, spongy-like structure. Similarly, in Fig. 2c, the well-defined circular pores with thin inner pores surface and thin pores wall lead to a large surface area. When comparing the two biochars, variations in pore size can be observed. Larger biochar particles tend to have a more extensive porous structure and greater surface area. In contrast, the porous structure and surface area of smaller biochar particles appear to be significantly reduced or destroyed (Rabiee Abyaneh et al., 2024; Hummadi, 2021). The presence of lignocellulose materials can be confirmed by the increase in carbon weight percentage observed in the EDAX analysis (Meraj et al., 2024). This large carbon structure provides strong

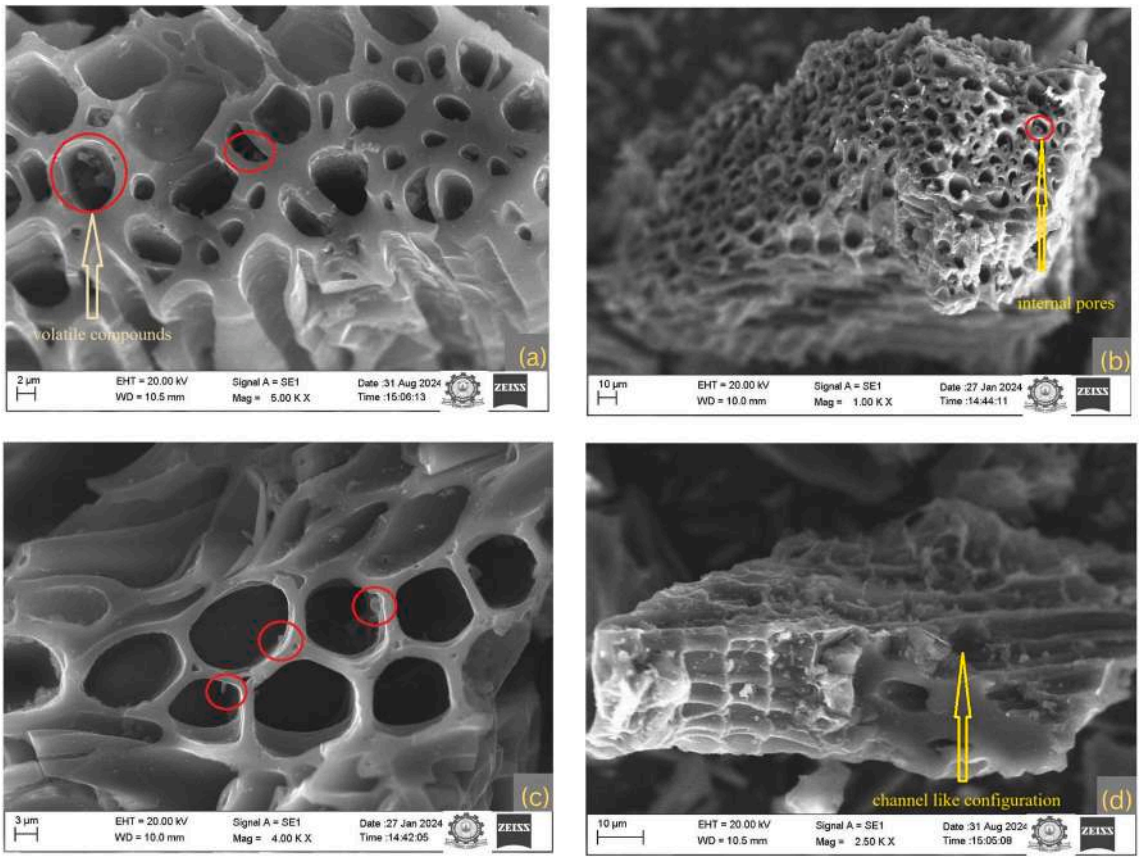

Fig. 2. (a) Picture depicts the volatiles in PJR400 biochar; (b) Picture b shows the interior pores in PJR400 biochar; (c) Volatiles and Internal pores are vanishing from PJR500 biochar; (d) There are tunnel-like holes in the PJR500 biochar.

capillary force to hold the molten paraffin within the matrix. By verifying the lignin and cellulose content in the biochar, the efficiency of the pyrolysis process can be assessed (Adeniyi et al., 2024). These morphological changes of biochar are what make the PCM a shape-stabilized material.

3.3. Bet surface area analysis

By employing N_2 adsorption and desorption techniques at 77K, BET (Brunauer–Emmett–Teller) analysis was used to ascertain the surface characteristics of the pure biochars. To guarantee accuracy, they were computed throughout a broad range of relative pressures, from $p/p_o = 0.01$ to $p/p_o = 0.99$. The surface area of pores, pore size, and pore size distribution are the most important parameters to determine the adsorption of biochar. The below Fig. 3 (a) shows that PJR 400 biochar exhibits a mesoporous shape due to multilayer adsorption at a relative pressure of 0.1 to 0.8. At saturation relative pressure, the adsorption peak increases, revealing a slightly macro porous structure. Since no elongation of the graph occurs at a relative pressure of 0.01, it is evident that there are no microspores. Similarly, PJR 500 biochar also confirms the mesoporous structure as shown in Fig. 3b. In this case, the absence of micro pores is confirmed as there is no growth of the graph at low relative pressure.

When the relative pressure exceeds 0.6, multilayer adsorption occurs, and capillary condensation begins. Furthermore, monolayer adsorption starts to take place at low relative pressure. According to the IUPAC classification, both biochars belong to Type IV due to mesoporous adsorption and capillary condensation (Eimontas et al., 2024). The average pore size of both biochars was studied using the Barrett-Joyner-Halenda (BJH) model. As shown in the below Fig. 3c and d, Particle size distribution (PSD) curve, a sharp peak appears at a pore size of 4–6 nm. This peak indicates that nitrogen gas adsorption occurs at a high level within this pore size range. This enables an accurate measurement of pore size. Similarly, as shown in Fig. 3d below, the graph of PJR500 increases from 3.9 nm to 5.1 nm, indicating significant multilayer adsorption.

The surface area, average pore size, and total pore volume of the two biochars are presented separately in Table 3 above.

This study demonstrates that as the pyrolysis temperature rises, pore size reduces while surface area and pore volume increase. As the temperature rises, volatile substances are removed from the porous structures, resulting in the formation of many pores. At higher temperatures, fluid molecules are removed from the porous structures of biochar, making it more brittle and degrading more quickly. Eventually, this action causes cracks to appear in the porous structure (Aziz et al., 2015; Claoston et al., 2014). Mesoporous and macro pores in biochar are known to have the capacity to absorb both liquids and solids (Shaaban et al., 2013; Downie et al., 2012). This study found that both biochars have the porosity necessary to absorb liquid PCM because of their mesoporous structure. PJR500 biochar has a greater volume and surface area than PJR400 biochar, suggesting a greater ability to absorb liquid PCM.

3.4. FTIR analysis of biochars

Using an IRTRACER-100 Shimadzu Fourier transform infrared spectroscopy (FTIR) analysis, the molecular composition and functional groups of both biochars were identified. This instrument operates over a wide spectral range of 7800-350 cm^{-1}, giving a maximum spectral resolution of 0.25 cm^{-1}. At the same time, studies were performed at an operating resolution of 4 cm^{-1} to ensure adequate signal quality and peak boundary. From below Fig. 4, the spectra of the two biochars were

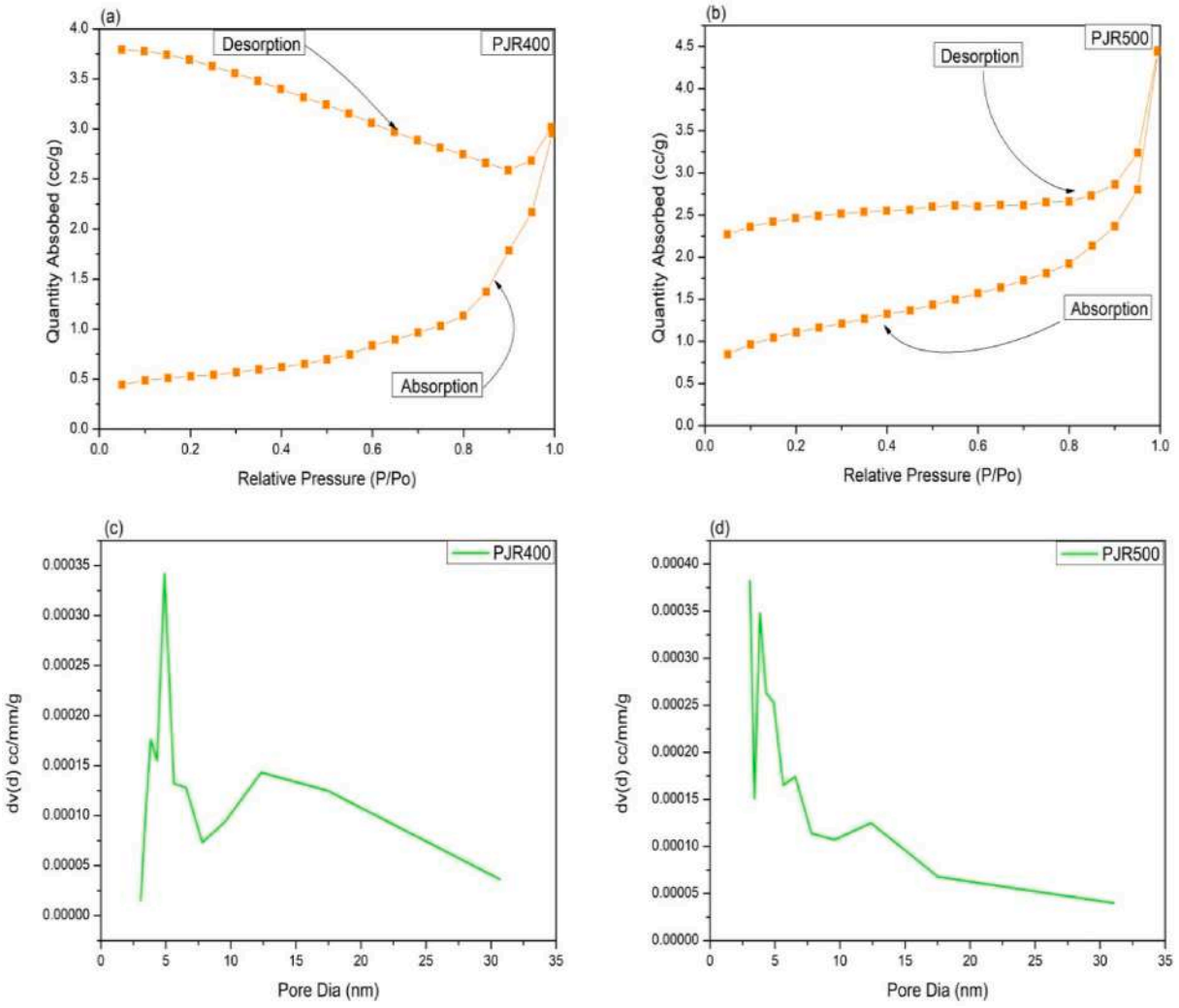

Fig. 3. (a) Graph for nitrogen gas absorption and desorption for PJR 400; (b) Graph for nitrogen gas absorption and desorption for PJR 500 biochar; (c) Pore size distribution (BJH) curve of PJR 400; (d) Pore size distribution (BJH) curve of PJR 500 biochar.

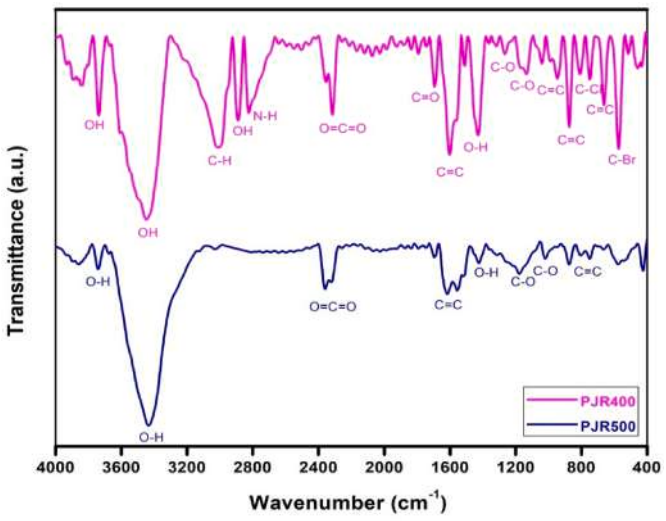

Fig. 4. PJR400 and PJR500 biochars' FTIR analysis.

different, with several peaks appearing, especially in the PJR400 fingerprint region. These spectra provide a good identification of the

Table 3
Study of specific surface area of Pores for all samples using BET.

S. No	Sample Code	BET Surface Area (m^2/g)	Average Pore Size (nm)	Total pore Volume (cc/g)
1	PJR500	4.451	6.2071	0.006907
2	PJR400	2.423	7.5710	0.004585

chemical components present. Additionally, in the case of PJR500, a significant reduction in the number of peaks in both the fingerprint and functional group regions was observed. This reduction is primarily due to the loss of volatile compounds as the temperature increases. The growth of clay, silicate and minerals is indicated by major peaks at 572 and 748 cm^{-1} in PJR400 biochar (Saikia et al., 2016).

Similar spectra are shown in the following PJR400 biochar. The C=C bending vibration of strong alkenes is observed at peak position 947,873,803 cm^{-1} (Singh et al., 2018). The O-H bending vibration at wavenumber 1429 cm^{-1} clarifies the formation of the Carboxylic acid (Liu et al., 2015). The high presence of alkyl aryl ether is indicated by the C-O stretching vibration seen at a wavenumber of 1265 cm^{-1}. This peak indicates that biochar contains significant amounts of components such as cellulose, hemicellulose, and lignin. The C=C asymmetric medium peak at 1602 cm^{-1} proves that lignin has formed (Armynah et al., 2018). The O=C=O stretching vibration at peak 2316 cm^{-1} indicates the

creation of strong alkyne and carbonyl bonds. The formation of this peak mainly shows that CO_2 gas can be absorbed by biochar (Cole et al., 2019). Peak position 2289 has alkane and aliphatic types with a medium C-H group. The occurrence of a hydroxyl group by hydrogen is shown by the peaks at 3008 and 3446 cm^{-1}, which are confined by the strong -OH stretching vibration and the CH_2 stretching vibration, respectively (Mccall et al., 2025). Its phenolic and alcoholic chemical characteristics are indicated by its peak location at 3758 cm^{-1}. Similarly, in PJR500, the functional groups such as alcohol and phenolic functional groups at 3741 cm^{-1}, hydrogen-bonded hydroxyl group at 3433 cm^{-1}, C=C asymmetry stretching vibration at 1616 and 1556 cm^{-1}, broad C-O stretching vibration at 1178 cm^{-1}, and silicate formation at 424 cm^{-1} receive major attention. However, if there are too many functional groups, there is a possibility of increased oxidation and a decrease in the stability of the carbon (Adhikari et al., 2024). Both biochars have a strong -OH stretching vibration with high transmittance. This means that there is a high possibility of hydrogen bonding when added to another material (Dai et al., 2023). Additionally, the -OH molecules found in phenolic and alcohol may improve the composites' stiffness and flexibility (Zhang et al., 2019). Overall, the FTIR test confirms the successful modification of carbonaceous biochar with oxygen-containing functional groups, which is expected to further enhance the interfacial interactions with paraffin wax in the composition of the composites.

3.5. XRD study of biochar

All biochars were subjected to XRD analysis using Bruker Eco D8 Advance. At a step size of 0.02°, the diffraction patterns were collected over 2θ ranges from 10° to 80° from a scanning speed of 1° min^{-1}. The operating voltage and current were maintained at 40 kV and 30 mA respectively. The XRD peak at the conclusion of this investigation makes it evident which element is more prevalent. When comparing the two biochars, as Fig. 5 below illustrates, the sharp peak's intensity rises with temperature. This demonstrates that the crystal structure has increased. According to the below Table 4, the crystallinity of PJR400 is 34.1% while that of PJR500 is 37.31%. The amorphous structure starts to vanish as the temperature rises and eventually changes into a crystalline structure. The crystallinity pattern is indicated by the high-intensity sharp peak, whereas the amorphous formation is indicated by the low-intensity broad peak. The diffraction plane (002) is represented by the peak located between 20^0 and 30^0 (Samy et al., 2023). As seen in the image, this represents the carbon content. The existence of SiO_2 in biochar is confirmed by the strong peak at 26.7^0 (Zhao and Nartey, 2014). The tiny pore-like structure inside PJR400's porous structure is one factor contributing to the decrease in crystallinity. Major peaks in PJR500 were found at angles such as 22.86^0, 28.15^0, and 29.62^0. The formation of graphite is shown by the peak seen at 28.15^0 and the peak formed at 22.86^0 (Mohan et al., 2018). Likewise, in PJR400, the formation of graphite is indicated by the primary crystalline peak at angle 29.08^0. Finally, XRD results show that biochar produced by pyrolysis processes has a mostly amorphous appearance and minimal crystalline structures, demonstrating successful physical stabilization without changing its chemical phase.

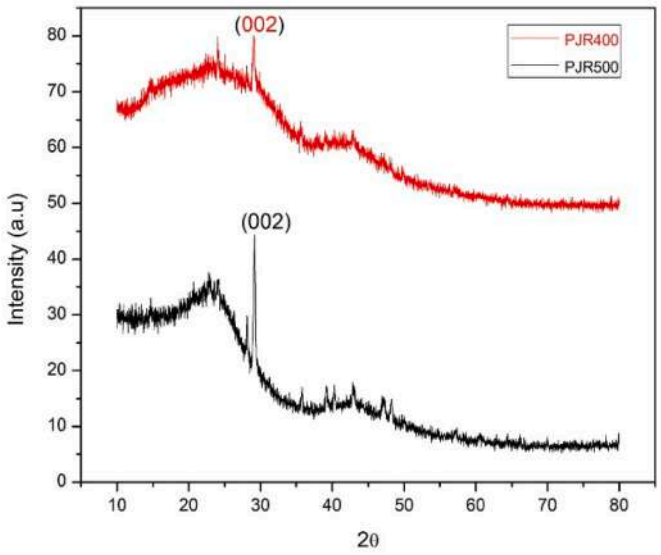

Fig. 5. Characterization of PJR400 and PJR500 biochar using XRD.

Table 4
Crystallinity and Amorphous percentages of PJR400 & PJR500 biochars.

S.NO	PJR400		PJR500	
	Crystalline %	Amorphous %	Crystalline %	Amorphous %
1	34.1	69.9	37.31	62.7

3.6. SEM analysis of PCM composites

The morphology of the shape-stabilized PCM composites, including surface structure and cross-sectional area, was examined using a Carl Zeiss EVO 18 scanning electron microscope at various magnifications. The PCM's entry into the porous structure is evident from these SEM pictures. For this study, the non-leaking PWPJR50045 composite and the leaking PWPJR50025 composite were taken and are shown in Fig. 6a–d, respectively.

It is evident from Fig. 6a that the PCM has fully penetrated the biochar's porous structure. Likewise, it is evident from the picture 6(b) that the PCM has not fully penetrated the biochar's skeleton. Similarly, the porous nature of the biochar without PCM filling is visible in the images 6c,d, at higher magnification. In certain areas, the PCM has deposited on the surface of the biochar without entering the porous structure. This is because of the partially filled porous structure and the potential for leakage from the surface area of the biochar covered with PCM. This might have an impact on the shape-stabilized PCM composites made from these PCM-covered biochars' thermal conductivity characteristics. It is known from these SEM experiments that particles with a fractured porous structure, particles with very small particle sizes, and particles that are not properly formed have poor bonding onto PCM.

3.7. XRD examination of PCM composites

XRD analysis of composites prepared with two types of biochar was carried out using Bruker Eco D8 Advance. From the results of the study, it was observed that there was no deviation in the elongation of the pure material compared to the elongation of the composites. Two major peaks of paraffin wax were observed at (2 theta) 21.74^0 and 24.11^0. These two peaks correspond to the crystal peaks of paraffin at 110 and 200 (Khan et al., 2020; Li et al., 2014). When compared to pure PCM, the peak intensity in both varieties of PCM composites is decreased. The crystallinity and amorphous percentage values of both PWPJR400 and PWPJR500 based PCM composites are given in the below Table 5. Biochar PJR500 with a higher crystallinity percentage achieves higher PCM adsorption.

At the same time, as PCM adsorption increases, the crystallinity percentage of the overall PCM composites decreases. Moreover, the peak intensity of PCM composites decreases as the amorphous percentage increases. The increase in amorphous structure and turbo static crystalline structure and the production of biochar at lower temperatures lead to the decrease in the peak intensity of PCM composites (Wu et al., 2012). Not only this, but there is also a possibility that the peak intensity additionally, as the weight percentage of biochar in PCM increases, the peak intensity falls. Fig. 7a and b illustrates how the peaks of PWPJR500

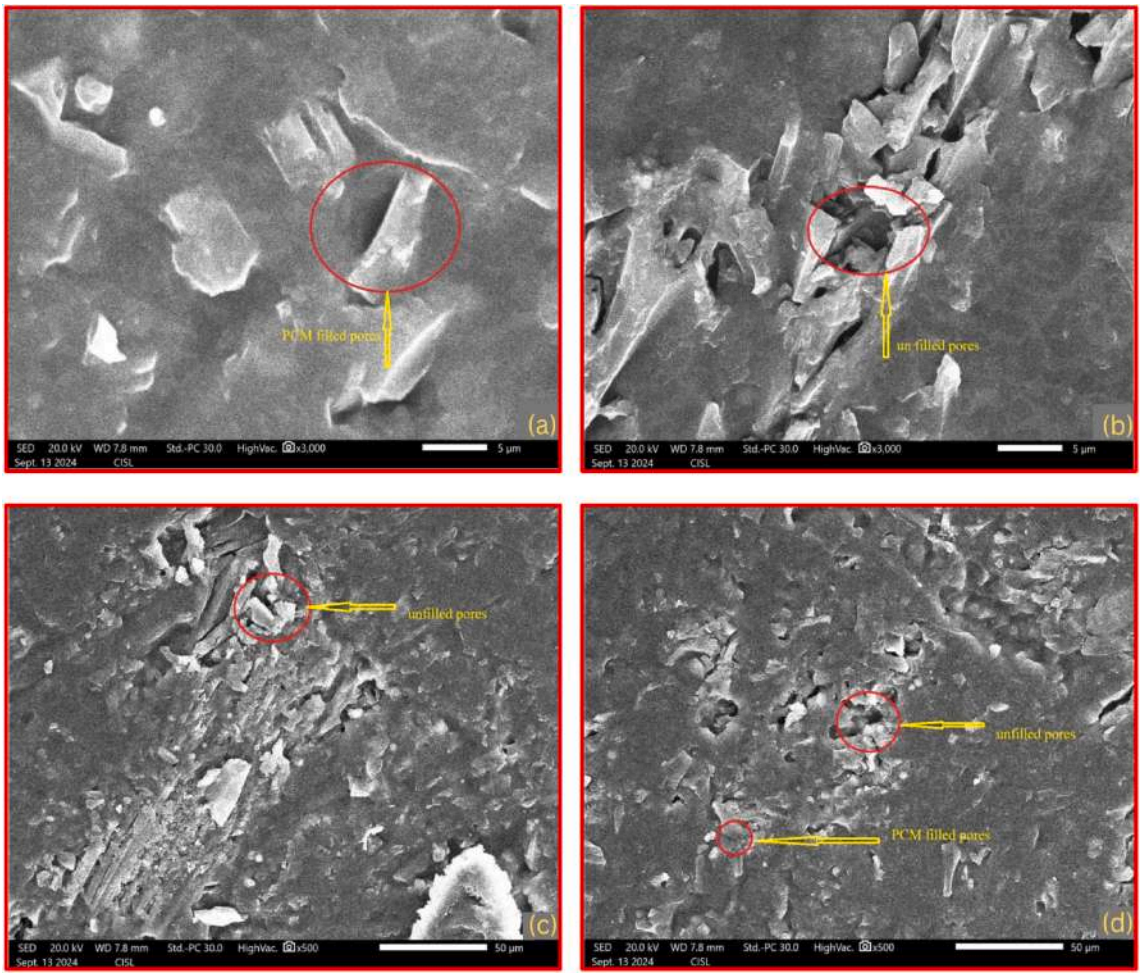

Fig. 6. (a) PCM that has penetrated deep into the hole may be seen in PWPJR50045; (b) Holes not covered by PCM are visible in PWPJR50045; (c) Uncovered holes and fractured channels can be observed in PWPJR40025; (d) There are numerous holes that are not closed with PCM, resulting in leakage in PWPJR40025.

Table 5
Crystalline and amorphous percentage values of all biochar-based PCM composites through XRD analysis.

S.NO	PWPJR400			PWPJR500		
	Sample Code	Crystalline %	Amorphous %	Sample Code	Crystalline %	Amorphous %
1	PW0	68.6	31.4			
2	PWPJR4005	67.4	32.4	PWPJR5005	63.1	36.9
3	PWPJR40015	60.8	39.2	PWPJR50015	55.2	44.8
4	PWPJR40025	59.8	40.2	PWPJR50025	54.9	45.1
5	PWPJR40035	59.0	41.0	PWPJR50035	54.6	45.4
6	PWPJR40045	58.8	41.2	PWPJR50045	53.6	46.4

composites are substantially smaller than those of PWPJR400 composites. The decrease in these peaks indicates that the PCM penetrated more into the PJR500 biochar than into the PJR400 biochar. Furthermore, the decrease in peak intensity indicates that PJR500 biochar, which has a high surface of PCM composites, may decrease due to the hydrogen bonds formed between PCM and biochar (Wan et al., 2019; Wang et al., 2012).

3.8. FTIR analysis of each PCM composite sample

FTIR analyses were carried out on all PCM mixes in order to look into the functional group and assess the changes following the addition of biochar. The spectra were recorded using a Shimadzu IRTracer-100 FTIR spectrometer, which has a high sensitivity infrared scanning range. Looking at the two Fig. 8(a) and ,(b), the spectra of the two biochar PCM blends show the same wavelength. The strong peak formed at 2914 and 2846 cm^{-1} wavenumbers indicates C-H stretching vibration. This shows the formation of strong alkanes and a small amount of aromatic compounds. As a result of alkanes, we can feel the presence of hydrocarbons, the main component of paraffin. Due to the high content of alkanes, phase segregation is likely to occur in PCM (Sharshir et al., 2023). Not only this, alkanes reduce the stiffness and flexibility of PCM and also have the potential to become brittle (Online, 2022). The peak at 1463 cm^{-1} indicates the formation of the functional group C-H scissoring methylene (Cushman et al., 2025). In the fingerprint region that describes the molecular structure, wave number 721 cm^{-1} represents the C-O bending vibration. When comparing the spectra of biochar PCM composites with the spectra of PCM from the two images below, there is no deviation, and no new spectrum is formed. Moreover, the peak intensity remains unchanged for all the samples. Finally, it can be said

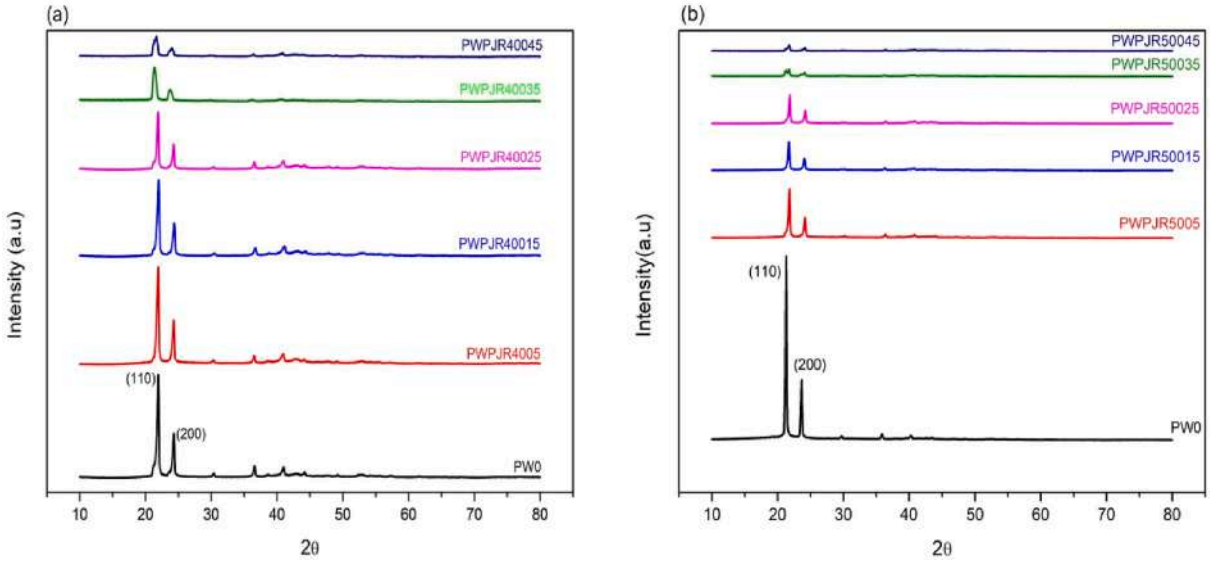

Fig. 7. (a) Characterization of PWPJR400PCM Composites; (b) Characterization of PWPJR500PCM composites using XRD.

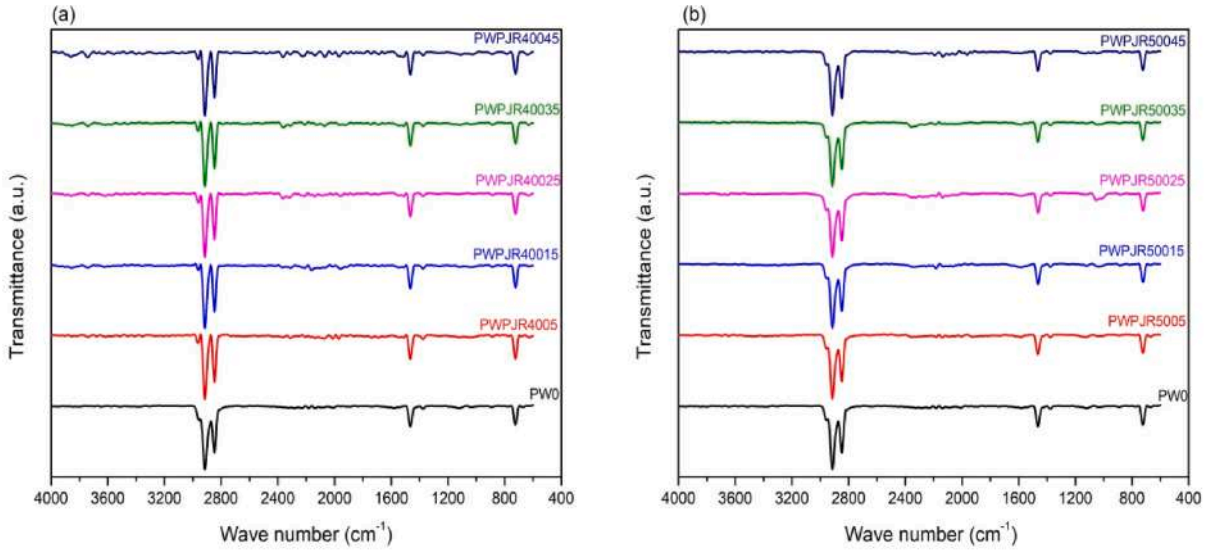

Fig. 8. (a) Peaks in the FTIR spectra of PWPJR400 PCM composites based on PJR400 biochar; (b) Peaks in the FTIR spectra of PWPJR500 PCM composites based on PJR500 biochar.

with certainty through FTIR analysis that there is no chemical reaction and no new polymer chain formation after mixing biochar with the PCM.

3.9. Assessing the thermal stability of PCM composites

Knowing the degradation temperature is one of the important things to know for using PCM in its applications. The degradation temperature values of PCM and PCM composites were determined by thermogravimetric analysis (TGA 4000) using a PerkinElmer instrument. The TGA analysis was performed from 30 °C to 500 °C for PCM, PCM composites, and biochar. The heating rate was taken at 10 °C/min in the presence of nitrogen gas supplied at 20 ml/min. As shown in Table 6, PJR400 biochar started degradation at 114 °C and PJR500 biochar at 156 °C. Degradation is normal at temperatures between 100 °C and 200 °C due to the decomposition of hydrated compounds and the evaporation of water molecules (Kim and Hadigheh, 2024; Hossain et al., 2009). Fig. 9a and b, degradation graphs for both biochars were parallel and linear. There is no abrupt decrease in the degradation peak at any temperature.

Table 6
Degradation and weight loss percentage for PJR400 and PJR500 biochars.

S. No	Sample Code	Degradation Temp (^{0}C)	Weight Loss % Up to 500 °C (%)	Weight percentage of the residual material after a temperature of 500 °C. (%)
1	PJR400	114	10.23	89.77
2	PJR500	156	6.27	93.73

Hemicellulose degrades at temperatures between 200 °C and 300 °C, cellulose at 250 °C and 380 °C, and lignin at 200 °C and 1000 °C (Hekimoğlu et al., 2021; Sarı, 2014). This is because hemicellulose and cellulose are gradually removed from the biochar at 200 °C, resulting in a consistent weight loss. However, both biochars do not show a dramatic degradation curve at 500 °C. This suggests that the primary components of biochar, lignin and cellulose, are stable at temperatures up to 500 °C. For this reason, up to 500 °C, biochar PJR400 lost 11.6% of its weight,

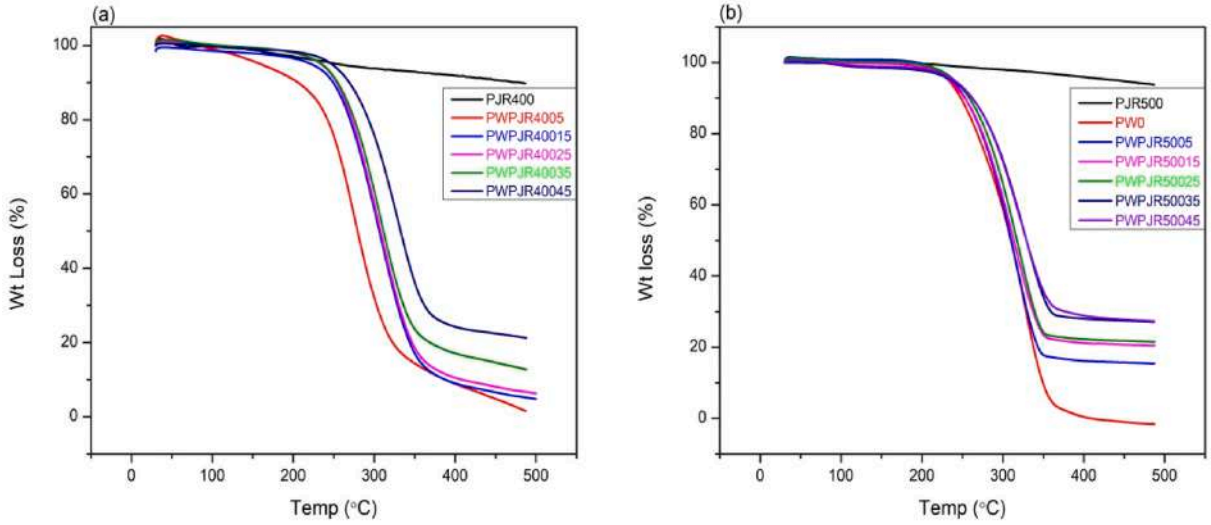

Fig. 9. (a) TGA diagram for PWPJR400 PCM composites and PJR400 biochar; (b) PJR500 biochar and associated PWPJR500 PCM composites TGA chart.

while PJR500 biochar lost only 7.2%. The figure above. 9a,b depict the single-step degradation curves for PCM and PCM blends. As shown in the figures, in PCM blends prepared with both types of biochar, the weight loss percentage decreases, but the residue percentage increases as the weight percentage of biochar in the PCM increases. If the residue % is higher, it can be inferred that the blend has better thermal stability (Liu and Peng, 2022). Since PWPJR500 has a higher residue percentage, this type of PCM blend has higher thermal stability. As Table 7 above illustrates, PWPJR500 type blends have higher residue percentage and lower weight loss percentage compared to other PWPJR400 type PCM blends. Therefore, PCM blends formed from biochar produced at high temperatures show higher thermal stability than those formed from biochar produced at low temperatures. However, paraffin wax starts to break down above 242 °C. Looking at Table 8 above, among the PWPJR400 PCM blends, only the PWPJR40045 blend has a higher decomposition temperature than pure paraffin wax. All other PWPJR400 blends have a lower decomposition temperature than pure paraffin wax. This is due to the low surface area and pore size of the PJR400 biochar and the inability to remove oxygen and volatiles from the porous structures, which prevents the PCM from entering the porous structures of the PCM biochar. Since the PCM does not enter the porous structure, the area is filled with volatiles and oxygen, which will increase the combustion process. Due to this reason, the decomposition of the composite PCMs decomposes earlier than the decomposition temperature of pure paraffin. The decomposition temperature of PCM and PCM blends is higher than the melting temperature used in applications where heat transfer can be controlled, so this study concludes that decomposition has no impact on the heat storage and heat release properties, which are the main properties of PCM and PCM blends.

Table 7
Degradation, weight loss, and residue values for shape-stabilized PCMs produced using PJR500 biochar.

S. No	Sample Code	Degradation Temp (^{0}C)	Final Degradation Temp (^{0}C)	Weight Loss %	Residue %
1	PW0	242.56	371.87	100	0
2	PWPJR5005	243.99	354.32	82.59	17.44
3	PWPJR50015	246.45	358.31	71.53	28.47
4	PWPJR50025	251.37	358.42	76.75	23.25
5	PWPJR50035	253.71	372	71.32	28.68
6	PWPJR50045	255.40	379.44	69.58	30.42

Table 8
Degradation, weight loss, and residue values for shape-stabilized PCMs made from PJR400 biochar.

S. No	Sample Code	Degradation Temp (^{0}C)	Final Degradation Temp (^{0}C)	Weight Loss %	Residue %
1	PWPJR4005	230.96	341.72	84.48	15.52
2	PWPJR40015	236.71	364.88	86.97	13.021
3	PWPJR40025	240.40	365.56	85.70	14.300
4	PWPJR40035	241.02	365.88	79.68	20.319
5	PWPJR40045	246.50	377.784	73.69	26.301

3.10. Assessment of heat capacity for storage

Values such as melting enthalpy, solidification enthalpy, melting point, and solidification temperature, which can reveal the heat storage and heat release properties of the compounds, were obtained using PerkinElmer (DSC 6000) differential scanning calorimetry. The results were analysed by the melting and solidification curves shown in Fig. 10a–d, In this study, heating temperature was given from 30 °C to 80 °C and cooling temperature from 80 °C to 30 °C according to the paraffin melting point temperature. The heating rate was 10 °C/min, and inert gas nitrogen was supplied at a rate of 20 ml/min. When looking at all the values in Tables 9 and 10, the enthalpy values of PWPJR500 PCM composites and PWPJR400 PCM composites have obtained much lower values than pure PCM. The latent heat enthalpy of melting and solidification enthalpy values of PCM composites decrease as the Weight percentage of biochar in PCM increases. However, the values in melting point temperature and solidification temperature fluctuate when compared with pure PCM. Especially when looking at the melting point temperatures of PWPJR500 types of composites given in below Table 10, only composites with high biochar weight start to decrease below the melting point temperature of pure PCM. For this, the long tunnel-like porous structure of biochar acts as a shield for PCM and the surface area of biochar acts as a bridge to conduct heat, leading to rapid heat transfer. As shown in Table 10, the onset melting temperature of the composites PWPJR50015, PWPJR50025, PWPJR50035, and PWPJR50045 is lower than that of pure PCM, and the onset solidification temperature is higher. This temperature change results in faster melting and solidification of the PCM composites than that of pure PCM. The unique carbon content of biochar and its properties, such as capillary action, surface tension, and constriction of space effect, enhance heat transfer within PCM composites (Hekimoğlu et al., 2021; Sarı,

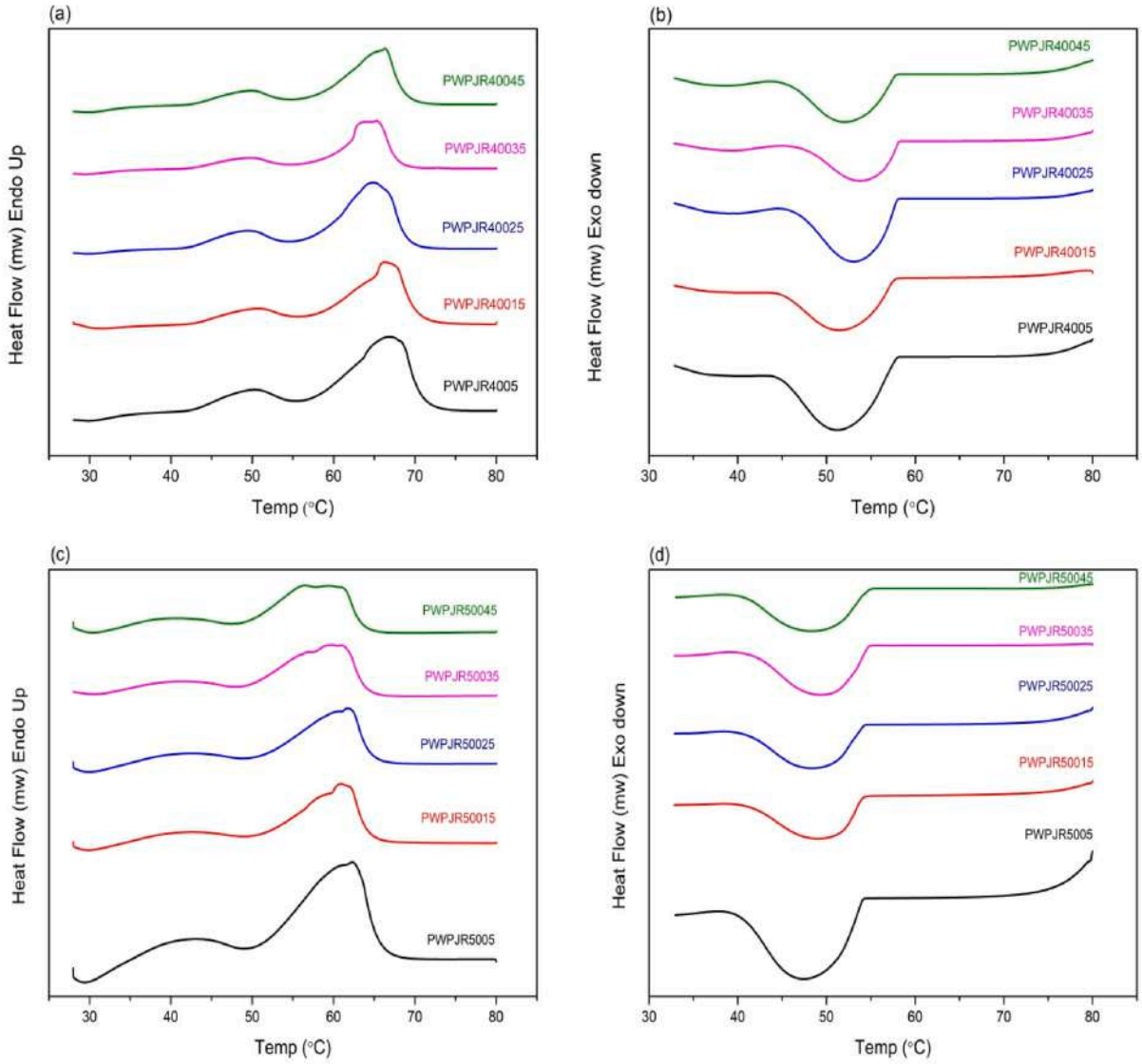

Fig. 10. (a) Melting enthalpy curves of PWPJR400 composites; (b) Solidification enthalpy curves of PWPJR400 composites; (c) Melting enthalpy curves of PWPJR500 composites; (d) Solidification enthalpy curves of PWPJR500 composites.

Table 9
The enthalpy, melting, and solidification temperatures of PCM composites made using PJR400 bio char from a DSC analysis.

S. no	Sample Code	Endothermic			Exothermic		
		Melting point Temp $(T_m)_{on}$ ^0C	Peak Temp (^0C)	Latent Heat Enthalpy of Melting (ΔH_m) J/g	Solidification Temp $(T_s)_{on}$ ^0C	Peak Temp (^0C)	Latent Heat Enthalpy of Solidification (ΔH_s) J/g
1	PWPJR4005	60.47	66.12	106.22	57.58	51.47	104.13
2	PWPJR40015	63.59	66.24	105.69	57.54	51.56	103.78
3	PWPJR40025	58.41	64.01	104.01	57.23	53.17	102.26
4	PWPJR40035	61.12	65.17	90.71	58.09	54.23	90.35
5	PWPJR40045	59.10	66.14	77.09	57.15	52.35	76.51

2014). Similarly, when looking at below Table 9, the melting point temperature and solidification temperature values of PWPJR400 PCM composites are found to be inconsistent. This is due to the fact that the PCM does not penetrate the porous structure properly and does not mix well with each other, resulting in agglomeration within the composites. Due to such reasons, changes in temperature have occurred. In this type of composite, the onset melting point temperature and peak melting point temperature are higher than that of pure PCM. This has delayed the melting of PCM. Due to this, biochar has become a thermal shield for PCM by preventing heat transfer. Furthermore, the latent heat enthalpy of melting values of all PCM composites and PCMs are higher than that of solidification values. In particular, the latent heat enthalpy of the solidification value of pure PCM is 2.65% lower than the latent heat enthalpy of the melting value. When the temperature drops to the melting point temperature of PCM, the stored heat is not completely released but is stored a little. On the other hand, when looking at PCM composites, the difference between the latent heat enthalpy of melting and the latent heat enthalpy of solidification values has decreased. The

Table 10
The DSC study enthalpy, melting, and solidification temperature results for PCM composites made with PJR500 biochar.

S. no	Sample Code	Endothermic			Exothermic		
		Melting point Temp (T_m) ^{0}C	Peak Temp (^{0}C)	Latent Heat Enthalpy of Melting (ΔH_m) J/g	Solidification Temp (T_s) ^{0}C	Peak Temp (^{0}C)	Latent Heat Enthalpy of Solidification (ΔH_s) J/g
1	PWPJR5005	56.76	60.94	95.46	54.00	49.49	92.78
2	PWPJR50015	51.57	62.25	87.03	54.06	47.69	86.08
3	PWPJR50025	51.48	61.79	77.50	54.03	48.66	76.37
4	PWPJR50035	49.84	61.00	76.60	54.44	49.49	75.02
5	PWPJR50045	49.63	59.85	70.24	54.64	48.49	68.53
6	PW0	51.76	58.25	170.02	54.02	49.46	165.62

difference between these two values has decreased due to the influence of biochar in PCMs. Thus, biochar has a significant impact on the heat storage and release properties of PCMs and increases the performance of PCMs. Similarly, the enthalpy values of shape stabilized PCM composites obtained by combining different biochar and PCM are given below. As stated by Liv et al., after 100 cycles, the melting and solidification enthalpies of polyethylene glycol (PEG) supported by pyrolyzed corn straw biochar (CSBC) were 100.2 J/g and 95.12 J/g, respectively (Liu and Peng, 2022). In accordance with Katish M. and associates, biochar PCM composite particles made using the vacuum impregnation technique during 300 thermal cycles displayed a latent heat of fusion of 116.7 J/g (Katish et al., 2024).

Li et al. and their colleagues reported that the mixture prepared by combining biochar derived from rice husk with n-octadecane showed a latent heat enthalpy of 128 J/g (Li et al., 2025). Xie T and his friends reported that combining tetradecanol with molten NaOH-Na2CO3-activated biochar yielded a latent heat enthalpy of 164.99 kJ/g (Xie et al., 2025). Bowei Du and his team reported that a polymethyl methacrylate-based microencapsulation PCM supporting material with a graphene oxide and carbon nanotube composite exhibited an enthalpy value of 165 J/g at a loading ratio of 67.7% (Du et al., 2026). Junlong Zou and his team reported that using copper foam as a supporting material, combined with paraffin RT 55, obtained an enthalpy value of 232.1 J/g (Zou et al., 2025). In our study, the 35% biochar PWPJR50035 composite had an enthalpy value of 76.60 J/g. However, when using non-biochar supporting materials such as carbon nanotubes and foams, the enthalpy values increase but are hampered by leakage and difficult preparation methods.

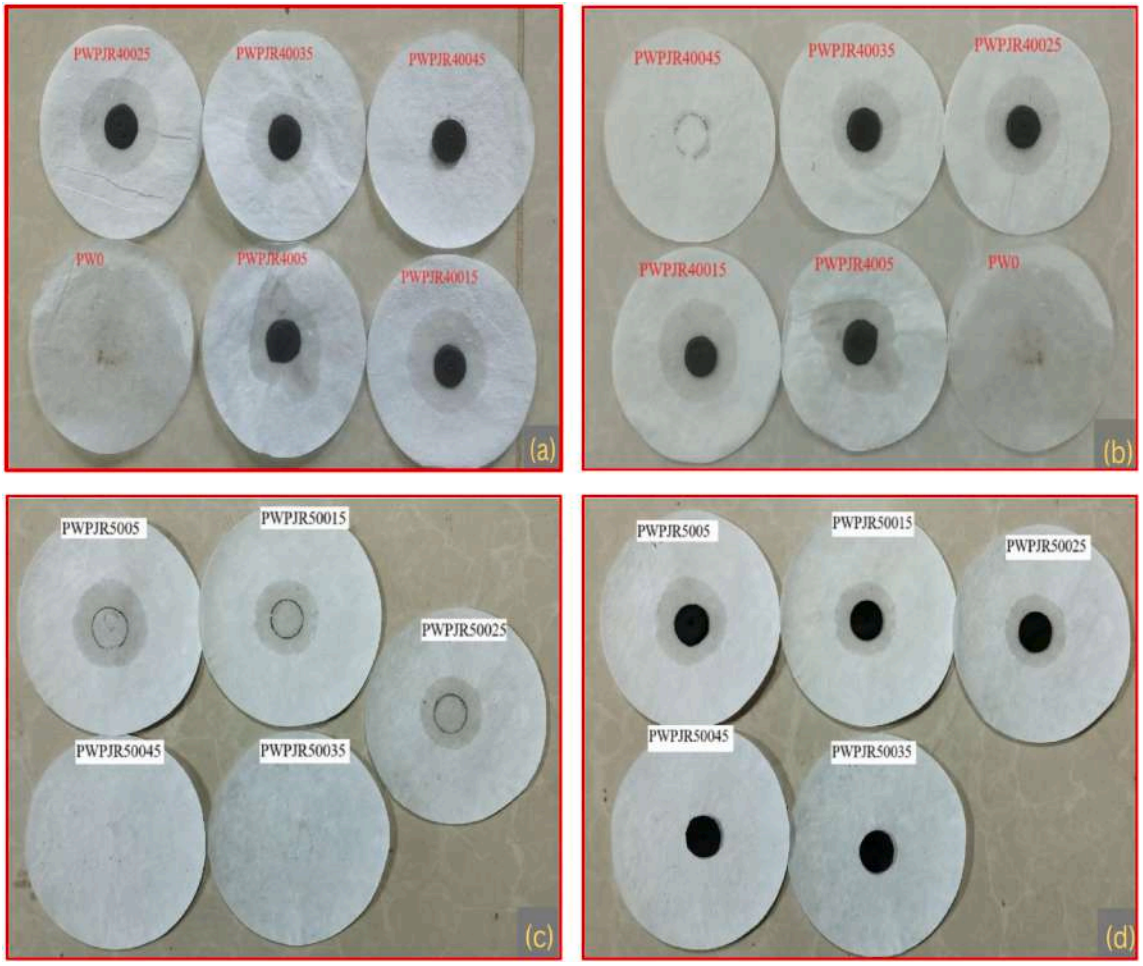

Fig. 11. (a) Evaluation of shape changes and leakage of PWPJR400 type PCM composites with sample at 80^{0}C; (b) Analysis of shape changes and leakage of PWPJR400 type PCM composites without sample at 80^{0}C; (c) Investigation of sample-free shape changes and leakage of PWPJR500 type PCM composites at 80^{0}C; (d) Inspection of shape changes and leakage of PWPJR500 type PCM composites with sample at 80^{0}C.

3.11. Results of PCM leakage test and all PCM composites

The leakage, an important property of pure PCM and shape-stabilized PCM composites, was investigated using Whatman filter paper. Circular samples of 21 mm diameter were placed in a high-temperature oven and maintained in an atmosphere of 80^0C, which is above the melting point temperature of PCM, for about 30 min. As shown in Fig. 11a and b, leakage was observed in all types of PWPJR400 composites based on the surface formed on the filter paper. The paraffin wax of PCM completely melted at a temperature of 80^0C and lost its shape and deposited as a surface on the filter paper. Then, the leakage intensity of the PCM composites formed with a lower biochar weight percentage increased and changes occurred in its shape. Leakage occurs because PCM is deposited on the surface of the biochar and does not effectively enter the porous structure. After the PCM, the PWPJR4005 sample with the lowest proportion of biochar exhibits the greatest leakage and shape change in this instance. At the same time, there is minimal weight loss and leakage when examining the PWPJR40045 sample with a high weight %. Likewise, as the picture illustrates 11c,d, the shape and extent of leakage have altered in the PWPJR500 PCM composites with a low proportion of biochar weight. But in the PWPJR50045 sample with a high percentage of biochar weight, there is absolutely no leakage. However, as shown in Fig. 11c and d, the PWPJR50035 sample has extremely minimal leakage. By the end of this study, the weight percentage of biochar has an impact on the PCM composites' leakage and shape change. Therefore, structure and leakage is affected when half or slightly less than half of the weight percentage of biochar is added to the weight percentage of PCM. Moreover, leakage was only avoided by the PCM composite composed of PJR500 biochar, which has a large surface area and pore volume. Consequently, a key factor in stopping PCM leakage is the porous structure of the supporting materials.

3.12. Inspection of thermal conductivity

Rapid heat transfer can significantly change the heat storage and release properties of PCMs. By increasing the heat transfer rate, the efficiency of PCMs can be enhanced when instantaneous cooling and melting occur. Rapid heat transfer depends on thermal conductivity. In this study, thermal conductivity and thermal effusivity values were measured separately for both biochar and PCM composites.

For this, thermal conductivity and thermal effusivity values were determined using a C-therm thermal conductivity analyser with ASTM D7984 standard. In this study, samples with a diameter of 21 mm and a thickness of 3 mm were tested at 27^0C using the MTPS method. Depending on the thermal conductivity value of composite materials, heat energy storage and release be varying. As shown in the above Table 11, biochar prepared at 500^0C has higher thermal conductivity and effusivity values than biochar prepared at 400^0C. It is clear from Fig. 12 (a) that the thermal conductivity and emissivity values increase as the temperature of the pyrolysis process increases. This is due to the destruction of volatile compounds that inhibit heat conduction and an increase in the weight percentage of minerals that can increase thermal conductivity. Based on the results obtained from the EDAX study, thermal conductivity and effusivity values increased in biochar with a higher carbon %. By maximizing heat transport, the carbon content raises thermal conductivity and effusivity. Not only is this, but the graphitization pattern created by the increase in crystallinity percentage also a reason for the increase in the thermal conductivity value. When compared to all other PCM composites, the PWPJR50045 composite with the highest weight percentage of biochar has the highest thermal conductivity and thermal effusivity values, as seen in the below Fig. 12b and c, In comparison to the pure PCM, the PWPJR50045 composite exhibits effusivity and thermal conductivity values that are 18.74% and 74.71% higher, respectively. The thermal conductivity and effusivity values of the two varieties of biochar PCM composites rise steadily as the weight percentage of biochar in the PCM increases. However, as the below Fig. 12b and c, illustrates, for every percentage of biochar weight, the PWPJR500 composites perform better than the PWPJR400 composites in terms of effusivity and thermal conductivity values. Self-vibration and electron mobility allow biochar to transmit heat across locations within the PCM (Prabhu et al., 2024; Dahal et al., 2019). Furthermore, biochar must have its own region within the PCM to vibrate without being arrested. Therefore, the thermal conductivity value will begin to drop if the biochar is halted and unable to vibrate in the PCM environment.

Similarly, the thermal conductivity values reported by other studies are presented below. In comparison to pure PCM, Junhu Ho and his group found that employing double-layer graphene as a supporting material with stearic acid increased thermal conductivity by 42.3% (Hu et al., 2026). Migyang Sun and his team demonstrated that peanut shell biochar increased the thermal conductivity of stearic acid to 0.38 W $m^{-1}k^{-1}$ (Sun et al., 2024). According to Laiquan and his associates, paraffin wax's thermal conductivity increased by 27.3% when 5 wt% activated biochar was added (Lv et al., 2024a). Raja Mony and his colleagues reported that coconut shell biochar increased the thermal conductivity of pure A46 PCM to 77.27% (Rajamony et al., 2025). LVL et al. reported that 10 wt% biochar increased the thermal conductivity of paraffin from 0.293 to 0.366 W $m^{-1}k^{-1}$ (Lv et al., 2024b).

4. Conclusion

The primary findings of our investigation are as follows:

SEM and EDAX studies show that as temperature increases, volatile particles and moisture are removed from biochar, raising its carbon and mineral weight percentages. This results in improved thermal conductivity and faster heat transfer. Several peaks in the FTIR data disappear at higher biochar compositions. PWPJR500 experienced excessive PCM absorption, and the PWPJR50045 PCM composition had the lowest weight loss (73.69%) in TGA studies. The DSC studies of leak-free PWPJR50045 and PWPJR50035 revealed melting enthalpy values of 70.24 (J/g) and 76.60 (J/g). Even at 80 °C, no leakage was observed for PWPJR50045 in leakage tests, and PWPJR50035 also substantially reduced leakage. PJR500 biochar shows thermal conductivity and discharge values of 0.740 (w $m^{-1}k^{-1}$) and 1470.2 ($ws^{1/2}$ $m^{-2}k^{-1}$), higher than those produced at 400 °C. Similarly, the PWPJR50045 mixture shows higher diffusivity and thermal conductivity values of 775.68 ($ws^{1/2}$ $m^{-2}k^{-1}$) and 0.414 (w $m^{-1}k^{-1}$) than the other mixtures.

Table 11
Values for the heat conduction and effusivity of all biochar and PCM composites.

S. No	Sample Code	Thermal conductivity (w $m^{-1}k^{-1}$)	Thermal effusivity ($ws^{1/2}$ $m^{-2}k^{-1}$)	Sample Code	Thermal conductivity (w $m^{-1}k^{-1}$)	Thermal effusivity ($ws^{1/2}$ $m^{-2}k^{-1}$)
1	PJR500	0.740	1470.29	PJR400	0.689	1402.67
2	PWPJR5005	0.309	690.24	PWPJR4005	0.294	690.31
3	PWPJR50015	0.324	712.02	PWPJR40015	0.321	706.81
4	PWPJR50025	0.388	748.75	PWPJR40025	0.344	731.17
5	PWPJR50035	0.414	775.68	PWPJR40035	0.396	763.24
6	PWPJR50045	0.463	796.85	PWPJR40045	0.420	778.97
7	PW0	0.265	670.57			

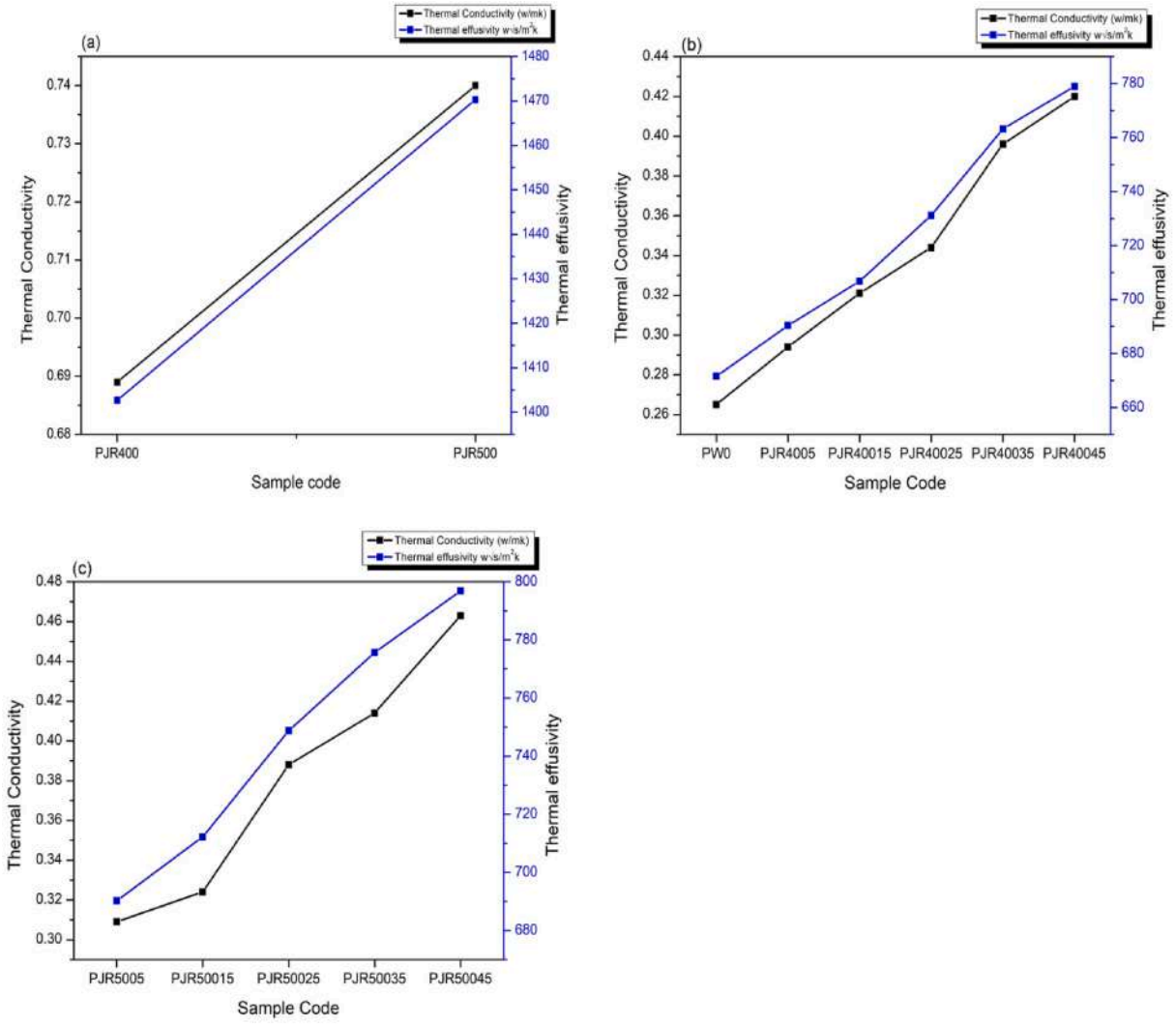

Fig. 12. (a) PJR400 and PJR500 biochar thermal conductivity and effusivity values; (b) PWPJR400 PCM composites thermal conductivity and effusivity values; (c) PWPJR500 PCM composites thermal conductivity and effusivity values.

These results indicate that pyrolysis temperature critically affects shape-stabilized PCM properties, including thermal conductivity, leakage, stability, and heat storage/release. Biochar produced by oxidative pyrolysis under inert gas can prevent PCM leakage and compete with inert-gas-pyrolyzed biochar in heat storage and release. A pyrolysis temperature of 500 °C and biochar weight percentages of 45% or 35% are especially important for preventing PCM leakage and improving thermal conductivity. Our study shows that PCM bio-composites, which are lightweight, stable, and leak-free, significantly improve the thermal comfort of solar heating products and electronic gadgets as construction materials.

Ethical approval

Not Applicable.

Availability of data and materials

Not Applicable.

Funding

Not Applicable.

CRediT authorship contribution statement

Karuppiah Theriselvam: Investigation, Methodology, Writing – original draft. **Arumugaprabu Veerasimman:** Conceptualization, Resources, Supervision, Validation, Writing – review & editing. **Flavio Stochino:** Conceptualization, Formal analysis, Funding acquisition, Resources, Supervision, Validation, Writing – review & editing. **Arnas Majumder:** Validation, Writing – review & editing.

Declaration of competing interest

On behalf of all the authors, we conclude that there is no conflict of interest.

Data availability

Data will be made available on request.

References

Adeniyi, A.G., Emenike, E.C., Ezzat, A.O., Iwuozor, K.O., Abd-Elkader, O.H., Al-Lohedan, H.A., et al., 2024. Investigating the properties and agronomic benefits of onion peel and chicken feather-derived biochars. Heliyon [Internet] 10 (15), e35485. https://doi.org/10.1016/j.heliyon.2024.e35485.

Adhikari, S., Moon, E., Paz-Ferreiro, J., Timms, W., 2024. Comparative analysis of biochar carbon stability methods and implications for carbon credits. Sci. Total Environ. 914 (October 2023), 169607. https://doi.org/10.1016/j.scitotenv.2023.169607 [Internet].
Agyenim, F., Hewitt, N., Eames, P., Smyth, M., 2010. A review of materials, heat transfer and phase change problem formulation for latent heat thermal energy storage systems (LHTESS). Renew. Sustain. Energy Rev. 14 (2), 615–628.
Amini, M.H.M., Temiz, A., Zuraik, M.A., Hermawan, A., Sulaiman, N.S., 2023. Shape stabilized phase change material by pine wood absorption. Mater. Today Proc.
Armynah, B., Atika, Djafar Z., Piarah, W.H., Tahir, D., 2018. Analysis of chemical and physical properties of biochar from rice husk biomass. J. Phys., Conf. Ser. 979 (1).
Arteconi, A., Hewitt, N.J., Polonara, F., 2012. State of the art of thermal storage for demand-side management. Appl. Energy 93, 371–389.
Asbik, M., Ansari, O., Bah, A., Zari, N., Mimet, A., El-Ghetany, H., 2016. Exergy analysis of solar desalination still combined with heat storage system using phase change material (PCM). Desalination 381, 26–37.
Asbik, M., Boushaba, H., Hafs, H., Koukouch, A., Sabri, A., Manokar, A.M., 2021. Investigating the effect of sensible and latent heat storage materials on the performance of a single basin solar still during winter days. J. Energy Storage 44, 103480.
Assareh, E., Keykhah, A., Hoseinzadeh, S., Astiaso Garcia, D., 2024. Application of PCM in a zero-energy building and using a CCHP system based on geothermal energy in Canada and the UAE. Buildings 14 (2).
Aydın, A.A., Okutan, H., 2013. Polyurethane rigid foam composites incorporated with fatty acid ester-based phase change material. Energy Convers. Manag. 68, 74–81.
Aziz, NS. binti A., Nor, MA. bin M., Manaf, SF. binti A., Hamzah, F., 2015. Suitability of biochar produced from biomass waste as soil amendment. Proced. Soc. Behav. Sci. 195, 2457–2465.
Bahadori, M.N., Haghighat, F., 1985. Weekly storage of coolness in heavy brick and adobe walls. Energy Build. 8 (4), 259–270.
Barzin, R., Chen, J.J.J., Young, B.R., Farid, M.M., 2015. Application of PCM underfloor heating in combination with PCM wallboards for space heating using price based control system. Appl Energy [Internet] 148, 39–48. https://doi.org/10.1016/j.apenergy.2015.03.027.
Boh, B., Šumiga, B., 2008. Microencapsulation technology and its applications in building construction materials Tehnologija mikrokapsuliranja in njena uporaba v gradbenih materialih. RMZ Mater. Geoenviron 55 (3), 329–344.
Bose, S., Kirk, R.D., Maslen, H., Islas, M.A.P., Smith, B., Dugmore, T.I.J., et al., 2022. RSC Advances Carbons Prepared from Degreased Spent Co Ff Ee Grounds for E Ffi Cient Removal of Mno 42 À in Aqueous Media, pp. 19417–19423.
Can, A., Žigon, J., 2022. N-heptadecane-impregnated wood as a potential material for energy-saving buildings. Forests 13 (12), 2137.
Claoston, N., Samsuri, A.W., Ahmad Husni, M.H., Mohd Amran, M.S., 2014. Effects of pyrolysis temperature on the physicochemical properties of empty fruit bunch and rice husk biochars. Waste Manag. Res. 32 (4), 331–339.
Cole, E.J., Zandvakili, O.R., Xing, B., Hashemi, M., Herbert, S., Mashayekhi, H.H., 2019. Dataset on the effect of hardwood biochar on soil gravimetric moisture content and nitrate dynamics at different soil depths with FTIR analysis of fresh and aged biochar. Data Br [Internet] 25, 104073. https://doi.org/10.1016/j.dib.2019.104073.
Costa, S.C., Kenisarin, M., 2022. A review of metallic materials for latent heat thermal energy storage: thermophysical properties, applications, and challenges. Renew. Sustain. Energy Rev. 154, 111812.
Cárdenas, B., León, N., 2013. High temperature latent heat thermal energy storage: phase change materials, design considerations and performance enhancement techniques. Renew. Sustain. Energy Rev. 27, 724–737.
Cushman, L., Zsiros, J., Kaeding, G., Bates, J., 2025. Chemical composition and properties of Ski wax: a comprehensive analysis of fluorinated, non-fluorinated, and bio-based waxes. Cold Reg. Sci. Technol. 230 (November 2024.
Dahal, R.K., Acharya, B., Saha, G., Bissessur, R., Dutta, A., Farooque, A., 2019. Biochar as a filler in glassfiber reinforced composites: experimental study of thermal and mechanical properties. Composites, Part B Eng. 175, 107169.
Dai, F., Zhuang, Q., Huang, G., Deng, H., Zhang, X., 2023. Infrared Spectrum Characteristics and Quantification of OH Groups in Coal.
Downie, A., Crosky, A., Munroe, P., 2012. Physical Properties of Biochar. Biochar for environmental management. Routledge, pp. 45–64.
Du, B., Jiang, X., Zhang, Z., Xi, K., Zhang, B., Yang, Q., et al., 2026. Graphene oxide/carbon nanotube reinforced PCM microcapsules with high thermal conductivity and high latent heat for thermal energy storage. Chem. Sci. 17 (1), 205–213.
Eimontas, J., Striūgas, N., Zakarauskas, K., Kiminaitė, I., Pitak, I., 2024. Metallised seaweed-derived bio-char catalyst preparation and its application in the pyrolysis process for the waste fishing nets and marine biomass utilisation. Fuel 357, 129922.
Farid, M., Khudhair, A.M., Razack, S.A.K., Al-Hallaj, S., 2021. A review on phase change energy storage: materials and applications. Therm Energy Storage with Phase Chang Mater 4–23.
Ge, H., Li, H., Mei, S., Liu, J., 2013. Low melting point liquid metal as a new class of phase change material: an emerging frontier in energy area. Renew. Sustain. Energy Rev. 21, 331–346.
Hashempour, S., Vakili, M.H., 2018. Preparation and characterisation of nano enhanced phase change material by adding carbon nano tubes to butyl stearate. J. Exp. Nanosci. 13 (1), 188–198.
Hekimoğlu, G., Sarı, A., Kar, T., Keleş, S., Kaygusuz, K., Yıldırım, N., et al., 2021. Carbonized waste hazelnut wood-based shape-stable composite phase change materials for thermal management implementations. Int. J. Energy Res. 45, 10271–10284.
Hossain, M.K., Strezov, V., Nelson, P.F., 2009. Thermal characterisation of the products of wastewater sludge pyrolysis. J. Anal. Appl. Pyrolysis 85 (1–2), 442–446.
Hu, J., Guo, Y., Gong, X., He, L., Yu, X., 2026. Thermal properties of graphene/stearic acid composite based on molecular dynamics. Int. J. Heat Mass Tran. 256, 127951.
Huang, B., Tu, P., Liang, J., Zhu, X., Deng, L., Hu, Z., et al., 2026. Synthesis of MgFe layered double hydroxide/biochar composite with satisfactory NH4+ adsorption via HPO42− intercalation. Ind. Crops Prod. 240, 122634.
Huang, J., Lu, S., Kong, X., Liu, S., Li, Y., 2013. Form-stable phase change materials based on eutectic mixture of tetradecanol and fatty acids for building energy storage: preparation and performance analysis. Materials 6 (10), 4758–4775.
Hummadi, K.K., 2021. Optimal operating conditions for adsorption of heavy metals from an aqueous solution by an agriculture waste. Iraqi J Chem Pet Eng 22 (2), 27–35.
Huynh, T.L., Dao, B.T.T., Le, M.T., Doan, K.A.T., Nguyen, T Do, Le, H.N., et al., 2026. Polyethyleneimine-modified activated biochar derived from rice husk ash: material development and preliminary formaldehyde adsorption study. Carbon Res. 5 (1), 5.
Iacomino, G., Idbella, M., di Costanzo, L., Amoroso, G., Allevato, E., Abd-ElGawad, A.M., et al., 2024. Biochar aging, soil microbiota and chemistry of charcoal kilns in mediterranean forests. Biochar [Internet] 6 (1). https://doi.org/10.1007/s42773-024-00378-3.
Jeon, J., Park, J.H., Wi, S., Yang, S., Ok, Y.S., Kim, S., 2019. Latent heat storage biocomposites of phase change material-biochar as feasible eco-friendly building materials. Environ. Res. 172, 637–648.
Kabeel, A.E., Sathyamurthy, R., Manokar, A.M., Sharshir, S.W., Essa, F.A., Elshiekh, A.H., 2020. Experimental study on tubular solar still using graphene oxide nano particles in phase change material (NPCM's) for fresh water production. J. Energy Storage 28, 101204.
Karaman, S., Karaipekli, A., Sarı, A., Biçer, A., 2011. Polyethylene glycol (PEG)/diatomite composite as a novel form-stable phase change material for thermal energy storage. Sol. Energy Mater. Sol. Cells 95 (7), 1647–1653.
Katish, M., Allen, S., Squires, A., Ferrandiz-mas, V., 2024. Experimental study of phase change material (PCM) biochar composite for net-zero built environment applications. Clean Mater [Internet] 14 (October), 100274. https://doi.org/10.1016/j.clema.2024.100274.
Khan, A., Saikia, P., Saxena, R., Rakshit, D., Saha, S., 2020. Microencapsulation of phase change material in water dispersible polymeric particles for thermoregulating rubber composites—A holistic approach. Int. J. Energy Res. 44 (3), 1567–1579.
Kim, D., Hadigheh, S.A., 2024. Oxidative pyrolysis of biosolid: air concentration effects on biochar formation and kinetics. Renew Energy [Internet] 224 (January), 120106. https://doi.org/10.1016/j.renene.2024.120106.
Kousksou, T., Bruel, P., Cherreau, G., Leoussoff, V., El Rhafiki, T., 2010. PCM storage for solar DHW: from an. In: 9th IIR Conference on Phase Change Materials and Slurries for Refrigeration and Air Conditioning, pp. 89–95.
Köse, G., 2023. N-octadecane/bio-char composite: preparation, characterization and energy storage properties. Mobilya ve Ahşap Malzeme Araştırmaları Derg 6 (2), 245–255.
Li, C., Sun, Z., Shao, J., Xu, H., Guo, C., Zhu, J., et al., 2025. A novel biochar supported dual-flame-retardant composite phase change material (PCM) for building energy saving. Constr. Build. Mater. 485, 141953.
Li, Y., Samad, Y.A., Polychronopoulou, K., Alhassan, S.M., Liao, K., 2014. From biomass to high performance solar-thermal and electric-thermal energy conversion and storage materials. J Mater Chem A. 2 (21), 7759–7765.
Liu, Y., He, Z., Uchimiya, M., 2015. Comparison of biochar Formation from various agricultural By-Products using FTIR spectroscopy. Mod. Appl. Sci. 9 (4), 246–253.
Liu, S., Peng, S., 2022. RSC Advances E Ff Ects of Biochar Pyrolysis Temperature on Thermal Properties of Polyethylene Glycol/Biochar Composites as shape-stable Biocomposite Phase, vols. 9587–98.
Liu, S., Yang, H., 2015. Composite of coal-series kaolinite and capric–lauric acid as form-stable phase-change material. Energy Technol [Internet] 3 (1), 77–83. Available from: https://onlinelibrary.wiley.com/doi/abs/10.1002/ente.201402125.
Liu, S., Yang, H., 2016. Porous ceramic stabilized phase change materials for thermal energy storage. RSC Adv. 6 (53), 48033–48042.
Lucas, S.S., Ferreira, V.M., Aguiar, JLB De, 2013. Latent heat storage in PCM containing mortars - study of microstructural modifications. Energy Build. 66, 724–731.
Lv, L., Huang, S., Zhou, H., 2024a. Effect of introducing chemically activated biochar as support material on thermal properties of different organic phase change materials. Sol Energy Mater Sol Cells [Internet] 264, 112617. Available from: https://www.sciencedirect.com/science/article/pii/S0927024823004385.
Lv, L., Huang, S., Zhou, H., 2024b. Performance investigation of biochar/paraffin composite phase change materials in latent heat storage systems: feasibility of biochar as a thermal conductivity enhancer. J Energy Storage [Internet] 91, 112106. Available from: https://www.sciencedirect.com/science/article/pii/S2352152X2401692X.
Mandal, S., Ishak, S., Lee, D.E., Park, T., 2022. Shape-stabilized orange peel/myristic acid phase change materials for efficient thermal energy storage application. Energy Rep. 8, 9618–9628.
Mandal, S., Mendhe, A.C., Park, T., Lee, H.S., 2026. Temperature-modulated surface features of neem seed biochar for sustainable thermal energy storage applications. Biochar 8 (1), 9.
Mccall, M.A., Watson, J.S., Tan, J.S.W., Sephton, M.A., 2025. Biochar Stability Revealed by FTIR and Machine Learning.
Mehling, H., Cabeza, L.F., 2008. Heat and cold storage with PCM. Heat mass Transf 11–55.
Meraj, A., Jawaid, M., Singh, S.P., Nasef, M.M., Ariffin, H., Fouad, H., et al., 2024. Isolation and characterisation of lignin using natural deep eutectic solvents pretreated kenaf fibre biomass. Sci Rep [Internet] 1–16. https://doi.org/10.1038/s41598-024-59200-6.

Mesnage, M., Omn, R., Colin, J., Ramezani, H., Jeong, J., 2025. Porous Biochar for Improving the CO $_2$ Uptake Capacities and Kinetics of Concrete, p. 157. October 2024).

Mohammed, M.A., Ali, B.M., Yassin, K.F., Ali, O.M., Alomar, O.R., 2024. Comparative study of different phase change materials on the thermal performance of photovoltaic cells in Iraq's climate conditions. Energy Rep. 11, 18–27.

Mohan, D., Abhishek, K., Sarswat, A., Patel, M., 2018. And Carbon Sequestration – a Sustainable Solution, pp. 508–520.

Murali, G., Ramani, P., Murugan, M., Elumalai, P.V., Ranjan Goud, N.U., Prabhakar, S., 2024. Improved solar still productivity using PCM and nano- PCM composites integerated energy storage. Sci Rep [Internet] 14 (1), 1–12. https://doi.org/10.1038/s41598-024-65418-1.

Noohi, Z., Nosouhian, S., Niroumand, B., Timelli, G., 2022. Use of low melting point metals and alloys (Tm $<$ 420 °C) as phase change materials: a review. Metals 12 (6).

Online, R., 2022. Designing and Characterization of Low-Temperature Eutectic Phase Change Materials Based on Alkanes.

Oya, T., Nomura, T., Okinaka, N., Akiyama, T., 2012. Phase change composite based on porous nickel and erythritol. Appl. Therm. Eng. 40, 373–377.

Pasupathy, A., Athanasius, L., Velraj, R., Seeniraj, R.V., 2008. Experimental investigation and numerical simulation analysis on the thermal performance of a building roof incorporating phase change material (PCM) for thermal management. Appl. Therm. Eng. 28 (5–6), 556–565.

Pomianowski, M., Heiselberg, P., Zhang, Y., 2013. Review of thermal energy storage technologies based on PCM application in buildings. Energy Build [Internet] 67, 56–69. https://doi.org/10.1016/j.enbuild.2013.08.006.

Prabhu, P., Jayabalakrishnan, D., Balaji, V., Bhaskar, K., Maridurai, T., Prakash, V.R.A., 2024. Mechanical, tribology, dielectric, thermal conductivity, and water absorption behaviour of Caryota urens woven fibre-reinforced coconut husk biochar toughened wood-plastic composite. Biomass Convers Biorefinery [Internet] 14 (1), 109–116. https://doi.org/10.1007/s13399-021-02177-3.

Qu, L., Li, A., Gu, J., Zhang, C., 2018. Thermal energy storage capability of polyurethane foams incorporated with microencapsulated phase change material. ChemistrySelect 3 (11), 3180–3186.

Rabiee Abyaneh, M., Nabi Bidhendi, G., Daryabeigi Zand, A., 2024. Pb(II), Cd(II), and Mn(II) adsorption onto pruning-derived biochar: physicochemical characterization, modeling and application in real landfill leachate. Sci Rep [Internet] 14 (1), 1–16. https://doi.org/10.1038/s41598-024-54028-6.

Rajamony, R.K., Chinnasamy, S., Kamaraj, R., Mohanthy, A., 2025. Thermal performance enhancement of phase change material using coconut shell biochar for sustainable thermal. Energy Storage 27 (3), 353–360.

Saeed, F.R., Mahmood, N.B., Jasim, M.A., 2022. One- dimensional numerical analysis for the porosity impact of open-cell metal foam on the effective thermal properties of PCMs, 9 (1).

Saffari, M., de Gracia, A., Fernández, C., Cabeza, L.F., 2017. Simulation-based optimization of PCM melting temperature to improve the energy performance in buildings. Appl. Energy 202 (c), 420–434.

Saikia, B.J., Parthasarathy, G., Borah, R.R., Borthakur, R., 2016. Raman and FTIR spectroscopic evaluation of clay minerals and estimation of metal contaminations in natural deposition of surface sediments from brahmaputra river, 2016 (July), 873–883.

Samy, M., Gar Alalm, M., abodlal, R.S., El-Dissouky, A., Khalil, M.N., El-Helow, E.R., et al., 2023. A novel corchorus olitorius-derived biochar/Bi12O17Cl2 photocatalyst for decontamination of antibiotic wastewater containing tetracycline under natural visible light. Sci Rep [Internet] 13 (1), 1–15. https://doi.org/10.1038/s41598-023-38715-4.

Sarı, A., 2014. Composites of polyethylene glycol (PEG600) with gypsum and natural clay as new kinds of building PCMs for low temperature-thermal energy storage. Energy Build. 69, 184–192.

Sarı, A., Saleh, T.A., Hekimoğlu, G., Tuzen, M., Tyagi, V.V., 2020. Evaluation of carbonized waste tire for development of novel shape stabilized composite phase change material for thermal energy storage. Waste Manag. 103, 352–360.

Shaaban, A., Se, S.M., Mitan, N.M.M., Dimin, M.F., 2013. Characterization of biochar derived from rubber wood sawdust through slow pyrolysis on surface porosities and functional groups. In: Procedia Engineering. Elsevier Ltd, pp. 365–371.

Sharshir, S.W., Joseph, A., Elsharkawy, M., Hamada, M.A., Kandeal, A.W., Elkadeem, M. R., et al., 2023. Energy & buildings thermal energy storage using phase change materials in building applications : a review of the recent development. Energy Build [Internet] 285, 112908. https://doi.org/10.1016/j.enbuild.2023.112908.

Singh, B., Fang, Y., Johnston, C.T., Science, E., Lafayette, W., 2018. HHS public access, 80 (3), 613–622.

Stonehouse, A., Abeykoon, C., 2022. Thermal properties of phase change materials reinforced with multi-dimensional carbon nanomaterials. Int. J. Heat Mass Tran. 183, 122166.

Sun, M., Feng, Y., Di, H., Lin, L., 2024. Evaluation into the effect of lignocellulosic biochar on the thermal properties of shape stable composite phase change materials. Ind Crops Prod [Internet] 222, 119961. Available from: https://www.sciencedirect.com/science/article/pii/S0926669024019381.

Sun, Z., Kong, W., Zheng, S., Frost, R.L., 2013. Study on preparation and thermal energy storage properties of binary paraffin blends/opal shape-stabilized phase change materials. Sol. Energy Mater. Sol. Cells 117, 400–407.

Wan, Y chao, Chen, Y., Cui, Z xing, Ding, H., Gao, S feng, Han, Z., et al., 2019. A promising form-stable phase change material prepared using cost effective pinecone biochar as the matrix of palmitic acid for thermal energy storage. Sci Rep [Internet] 9 (1), 1–10. https://doi.org/10.1038/s41598-019-47877-z.

Wang, C., Feng, L., Li, W., Zheng, J., Tian, W., Li, X., 2012. Shape-stabilized phase change materials based on polyethylene glycol/porous carbon composite: the influence of the pore structure of the carbon materials. Sol. Energy Mater. Sol. Cells 105, 21–26.

Wu, W., Yang, M., Feng, Q., McGrouther, K., Wang, H., Lu, H., et al., 2012. Chemical characterization of rice straw-derived biochar for soil amendment. Biomass and Bioenergy [Internet] 47 (December), 268–276. https://doi.org/10.1016/j.biombioe.2012.09.034.

Xiao, X., Zhang, P., Li, M., 2013. Preparation and thermal characterization of paraffin/metal foam composite phase change material. Appl. Energy 112, 1357–1366.

Xiao, X., Zhang, P., Li, M., 2014. Effective thermal conductivity of open-cell metal foams impregnated with pure paraffin for latent heat storage. Int. J. Therm. Sci. 81, 94–105.

Xie, T., He, J., Zhou, Z., Yu, S., Yan, T., Hu, H., et al., 2025. Synthesis and properties of shape-stabilized composite phase change material based on biochar via molten salt thermal treatment. Int. Commun. Heat Mass Tran. 169, 109782.

Zalba, B., Marín, J.M., Cabeza, L.F., Mehling, H., 2003. Review on thermal energy storage with phase change: materials, heat transfer analysis and applications. Appl. Therm. Eng. 23 (3), 251–283.

Zhang, Y., Ding, J., Wang, X., Yang, R., Lin, K., 2006. Influence of additives on thermal conductivity of shape-stabilized phase change material. Sol. Energy Mater. Sol. Cells 90 (11), 1692–1702.

Zhang, Y., Wen, G., Fan, S., Chu, Y., Li, S., Xu, B., et al., 2019. Phenolic hydroxyl functionalized partially reduced graphene oxides for symmetric supercapacitors with significantly enhanced electrochemical performance. J. Power Sources 435, 226799.

Zhao, B., Nartey, O.D., 2014. Characterization and evaluation of biochars derived from agricultural waste biomass from Gansu. In: China in Proceedings of the World Congress on Advances in Civil, Environmental, and Materials Research, Busan, Republic of Korea.

Zou, J., Ge, W., Hu, C., Fukuda, H., Meng, X., 2025. Case studies in thermal engineering effect of copper foam fin shapes on the thermal performance of spherical encapsulated phase-change material (PCM) in packed-bed latent heat storage system. Case Stud Therm Eng [Internet] 72 (May), 106390. https://doi.org/10.1016/j.csite.2025.106390.